Indian Journal of Pure & Applied Physics
Vol. 57, April 2019, pp. 236-249

Spectroscopic (FT-IR, FT-Raman and NMR) and NBO analysis of 3, 4-dimethylanisole by density functional method

S Manimaran[a], K Sambathkumar[b]*, N Rajkamal[c], M Venkatachalapathy[c] & K Chandrasekaran[b]

[a]P G & Research Department of Physics, Thanthai Hans Roever College (Autonomous), Perambalur 621 220, India

[b]P G & Research Department of Physics, A A Government Arts College, Villupuram 605 602, India

[c] P G & Research Department of Physics, Thiru AGovindasamy Government Arts College, Tindivanam 604 001 India

Received 19 July 2016; accepted 22 October 2018

Combined experimental and theoretical studies have been conducted on the molecular structure and vibrational, spectra of 3, 4-dimethyl anisole (DMA). The FT-IR and FT-Raman spectra of DMA have been recorded in the solid phase. The molecular geometry and vibrational frequencies of DMA in the ground state have been calculated by using the *ab-initio* Hartree-Fock (HF) and density functional methods (B3LYP) invoking 6-31+G (d,p) basis set. The optimized geometric bond lengths and bond angles obtained by HF method shows best agreement with the experimental values. Comparison of the observed fundamental vibrational frequencies of DMA with calculated results by HF and density functional methods indicates that B3LYP is superior to the scaled HF approach for molecular vibrational problems. The difference between the observed and scaled wave number values of most of the fundamental is very small. The thermodynamic functions and atomic change of the title compound has also been performed at HF/B3LYP/6-31+G(d,p) level of theories. A detailed interpretation of the FT-IR, FT-Raman, NMR spectra of DMA has also been reported. The theoretical spectrograms for infrared and Raman spectra of the title molecule have been constructed. The thermodynamic function of the title compound has also been performed at HF/6-31+G (d,p) and B3LYP/6-31+G (d,p) level of theories. Natural bond orbital analysis has been carried out to explain the change transfer or delocalization of change due to the intra-molecular interactions. Energy of the highest occupied molecular (HOMO) orbital and lowest unoccupied (LUMO) molecular orbital have been predicted.

Keywords: FTIR, FT-Raman, DMA, HOMO-LUMO, NBO, NMR

1 Introduction

Anisole is used in perfumery, chemical syntheses and an insect pheromone. Particularly *O*-nitro anisole is a bio-agent and it is mainly used to synthesize amino anisole, dyes and medicine. The application of nitro anisole as a detector for middle infrared interferometry[1] has been confirmed. Since the nitro anisole absorbs IR radiation heat it is possible to estimate the IR intensity distribution on the nitro anisole from the diffraction pattern made by visible larger light that is transmitted through it. It is used to measure the mono phenolase activity of polyphenol oxidize from fruits and vegetables[2]. Nitro anisole is a simple device which is used to detect mid-IR radiation. The nitroanisole exhibits a thermal lens effect[3-5], in which the refractive index is dependent upon temperature. This effect results in the phase modulation on visible light, in direct response to intensity of the incident IR radiation which is absorbed as heat. In the case of IR laser interferometry, interference fringe patterns that are created by the IR laser on the nitroanisole are observed as the refractive index distribution; hence the nitroanisole functions as a phase grating for visible light. It is, therefore, conceivable to estimate the IR intensity distribution on the nitroanisole by analyzing the diffraction pattern made by a visible laser, which is transmitted through the nitroanisole. Also, since a two dimensional device using the nitroanisole does not require matrix structure, it is expected that the measurement system must have high spatial resolution, equivalent to that of existing IR cameras. Owing to these applications and the reliable properties of anisole, a complete vibrational study on 3,4-dimethylanisole (DMA) has been undertaken. The vibrational analyses of DMA using the SQM force field method based on DFT calculation have been presented. The calculated infrared and Raman spectra of DMA are also simulated utilizing the computed dipole derivatives for IR intensities and polarizability derivatives for Raman activities.

*E-mail: sa75kumar@yahoo.co.in

2 Experimental Analysis

The solid sample of DMA obtained from Lancaster Chemical Company, UK was used as such for the spectral measurements. The Fourier transform infrared spectra of the title molecule are recorded in the region 4000 - 400 cm^{-1} on BRUKER IFS 66V model FTIR spectrometer equipped with an MCT detector, a KBr beam splitter and globar arc source. The spectrum is recorded at room temperature, with scanning speed of 30 cm^{-1} min^{-1} and the spectral resolution of ± 1 cm^{-1}. Boxcar apodization was used for the 250 averaged interferograms collected for both the sample and background. The FT-Raman spectrum of DMA is recorded on a computer interfaced BRUKER IFS66V model interferometer equipped with FRA-106 FT–Raman accessories. The sample is mounted in the sample illuminator using optical mount and no sample pretreatment of kind is undertaken. The spectrum is measured in the Stokes region 3500 - 50 cm^{-1} using Nd:YAG laser operating at 200 mW power continuously with 1064 nm excitation. The spectrum is recorded over 500 scans at a fixed temperature. The reported wave numbers are expected to be accurate within ± 1 cm^{-1}.

3 Computational Methodology

The entire calculations are performed at Hartree-Fock (HF) and density functional (DFT) levels using GAUSSIAN 09W [6] program package, invoking gradient geometry optimization[7]. Initial geometry generated from the standard geometrical parameters was minimized without any constraint on the potential energy surface at HF level adopting the standard 6-311++G(d,p) basis set. This geometry was then re-optimized again at DFT level employing the Becke 3LYP keyword, which invokes Becke's three-parameter hybrid method[8] using the correlation function of Lee *et al.*[9] implemented with the same basis set. The optimized structural parameters are used for the vibrational frequency calculations at DFT level to characterize all the stationary points as minima. The multiple scalings of the force constants are performed according to SQM procedure[10,11] using selective scaling in the natural internal coordinate representation[12,13]. The transformation of force field; subsequent normal coordinate analysis and calculation of the TED are done on a PC with MOLVIB program (version V7.0 – G77) written by Sundius[14-16]. By the use of GAUSSVIEW molecular visualization program[17] along with available related molecules; the vibrational frequency assignments are made by their TED with a high degree of confidence. The TED elements provide a measure of each internal co-ordinate's contributions to the normal coordinate.

The Raman activities (S_i) calculated with the GAUSSIAN 09W program are subsequently converted to relative Raman intensities (I_i) using the following relationship derived from the basic theory of Raman scattering[18-20]:

$$I_i = \frac{f(\nu_o - \nu_i)^4 S_i}{\nu_i \left[1 - \exp(-hc\nu_i / kT)\right]}$$

where ν_0 is the exciting frequency in cm^{-1}, ν_i the vibrational wave number of the i^{th} normal mode, h, c and k are the fundamental constants and f is a suitably chosen common normalisation factor for all the peak intensities.

4 Results and Discussion

4.1 Molecular geometry

The molecular structure of DMA belongs to C_1 point group symmetry. For C_1 symmetry there would not be any relevant distribution. The molecule consists of 22 atoms and expected to have 60 normal modes of vibrations of the same a species under C_1 symmetry. These modes are found to be IR and Raman active suggesting that the molecule possesses a non-centrosymmetric structure, which recommends the DMA for non-linear optical applications. The optimized molecular structure of DMA is shown in Fig. 1.

4.2 PES scan studies

The potential energy surface (PES) scan with the B3LYP/6-311++G(d,p) level of theoretical approximations was performed for DMA is shown in Fig. 2. The dihedral angle C5–C6–O18–C19 for DMA is also relevant coordinate for conformational

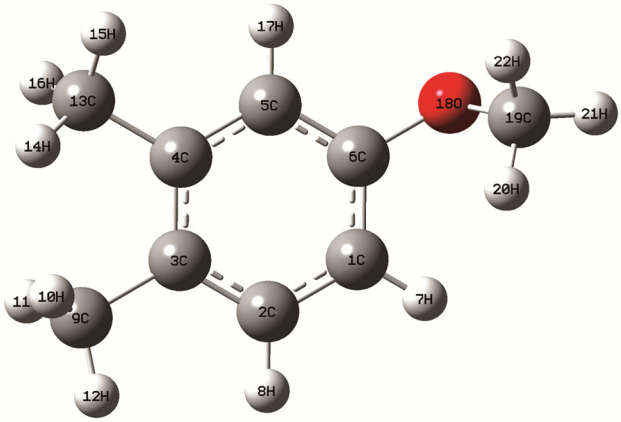

Fig. 1 — Molecular structure of 3,4-dimethylanisole.

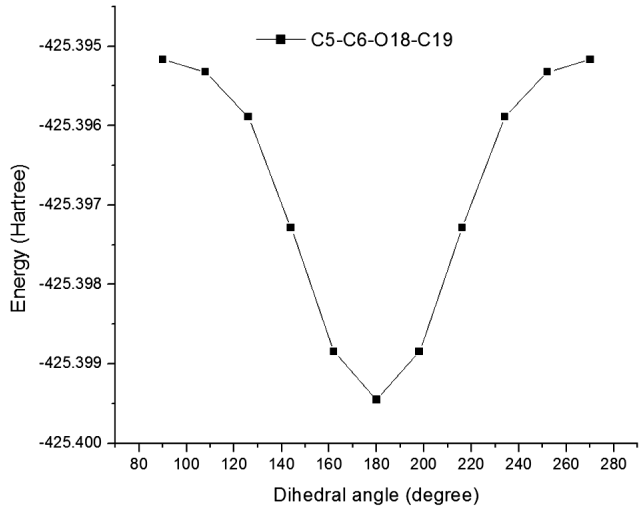

Fig. 2 — PES scan of 3,4-dimethylanisole.

flexibility within the molecule. During the calculation, all the geometrical parameters are simultaneously relaxed while the C5–C6–O18–C19 torsional angle are varied in steps of 10°, 20°, 30°,···, 360°. For this rotation minimum energy curves have been obtained at 0°, 110° and 250° as shown in Fig. 2 which clearly demonstrates that 0° corresponding to the global minimum energy is −425.39517016 Hartrees for DMA, and the minimum energy for the rotation at 110° and 250° are −425.39884271, −425.39532256 Hartrees for DMA. The maximum energy is obtained at 180° for both the molecules.

4.3 Structural properties

The optimization geometrical parameters of DMA obtained by the *ab initio* HF and DFT/B3LYP methods with 6-311++G(d,p) as basis set are listed in Table 1. The computed bond length and bond angles

Table 1 — Optimized geometrical parameters of 3,4-dimethylanisole by using B3LYP/6-311+G(d,p) and B3LYP/6-311++G(d,p) methods and basis set calculations.

Bond Length	Value (Å)		Exp	Bond Angle	Value (°)		Exp	Dihedral Angle	Value (°)	
	HF/6-311++G(d,p)	B3LYP/6-311++G(d,p)			HF/6-311++G(d,p)	B3LYP/6-311++G(d,p)			HF/6-311++G(d,p)	B3LYP/ 6-311++(d,p)
C1-C2	1.3885	1.3917		C2-C1-C6	119.1155	119.206		C6-C1-C2-C3	-0.1404	-0.0023
C1-C6	1.3806	1.3966		C2-C1-H7	120.9869	123.7324		C6-C1-C2-C8	-179.7758	179.9972
C1-H7	1.0752	1.0807	1.098	C6-C1-H7	119.8926	119.0616		H7-C1-C2-C3	179.0453	-180.002
C2-C3	1.3881	1.405		C1-C2-C3	121.8922	121.9414	1.079	H7-C1-C2-H8	-0.5901	-0.0025
C2-C8	1.0765	1.0834		C1-C2-H8	118.8704	119.0478		C2-C1-C6-C5	0.3983	0.0049
C3-C4	1.4025	1.4103		C3-C2-H8	119.2964	119.0108		C2-C1-C6-O18	178.4363	-179.993
C3-C9	1.512	1.5124		C2-C3-C4	118.6122	118.4419		H7-C1-C6-C5	-178.7965	180.0046
C4-C5	1.3884	1.4056		C2-C3-C9	120.2513	120.3481		H7-C1-C6-O18	-0.7585	0.0058
C4-C13	1.5116	1.5124		C4-C3-C9	121.1356	121.21		C1-C2-C3-C4	-0.1747	-0.004
C5-C6	1.3874	1.3969		C3-C4-C5	119.3327	119.6715		C1-C2-C3-C9	-179.8188	-179.994
C5-H17	1.076	1.081		C3-C4-C13	120.9047	12.7661		H8-C2-C3-C4	179.4594	-180.003
C6-O18	1.3641	1.3983	1.203	C5-C4-C13	119.7619	119.5625		H8-C2-C3-C9	-0.1847	0.0058
C9-H10	1.0864	1.0944	1.098	C4-C5-C6	121.1685	120.6826		C2-C3-C4-C5	0.2296	0.0077
C9-H11	1.0864	1.0943	1.098	C4-C5-H17	120.2937	118.674		C2-C3-C4-C13	-179.462	-179.982
C9-H12	1.836	1.0906	1.098	C6-C5-H17	118.5328	120.6424		C9-C3-C4-C5	179.8704	179.9982
C13–H14	1.0862	1.094	1.244	C1-C6-C5	119.8776	120.0556		C9-C3-C4-C13	0.1788	0.0077
C13-H15	1.0833	1.0905	1.244	C1-C6-O18	120.4297	115.7492	2.713	C2-C3-C9-H10	119.5713	120.0253
C13-H16	1.0862	1.094	1.244	C5-C6-O18	119.6638	124.1953		C2-C3-C9-H11	-120.4032	-120.066
O18-C19	1.4067	1.4513	1.091	C3-C9-H10	111.5946	111.9594		C2-C3-C9-H12	-4082	-0.0213
C19-H20	1.0861	1.0928	1.181	C3-C9-H11	111.6097	111.9552		C4-C3-C9-H10	-60.0637	-59.9651
C19-H21	1.081	1.0855	1.181	C3-C9-H12	11.7509	110.8345		C4-C3-C9-H11	56.9618	59.9436
C19-H22	1.0859	1.0928	1.181	H10-C9-H11	107.2787	106.802	1.080	C4-C3-C9-H12	179.9568	179.9883
				H10-C9-H12	107.7028	107.5173	1.080	C3-C4-C5-C6	0.0263	-0.0052
				H11-C9-H12	107.7071	107.5375		C3-C4-C5-H17	-179.1411	-180.005
				C4-C13-H14	111.3631	111.6663		C13-C4-C5-C6	179.7215	179.9854
				C4-C13-H15	110.9075	111.1722		C13-C4-C5-H17	0.5541	-0.0146
				C4-C13-H15	111.3913	111.6729		C3-C4-C13-H14	59.7731	59.7241

[a] For numbering of atoms refer Fig.1.
[a]Experimental values are taken from Ref.[21]

are compared with X-ray diffraction data of similar compound [21]. From Table 1, it can be seen that there are some deviations in the computed geometrical parameters from those reported in the single crystal XRD data, and these differences are probably due to the intermolecular interactions in the crystalline state. Comparing bond angles and bond lengths of B3LYP method with HF method, various bond lengths are found to be almost same at HF/6-311++G(d,p) and B3LYP/6-311++G(d,p) levels. However, the B3LYP/6-311++G(d,p) level of theory, in general slightly over estimates bond lengths but it yields bond angles in excellent agreement with the HF method. For the investigated molecule, the benzene ring appears a little distorted with larger C4–C5, C1–C2 bond length and shorter C1–C2, C4–C5 bond length and angles slightly out of the regular hexagonal structure for DMA and MNA. These distortions are explained in terms of the change in hybridisation affected by the substituent at the carbon site to which it is appended. The DMA of C–C bond lengths adjacent to the C2–C3, C19–O18 bonds increase and the angles C2–C1–C6, C2–C3–C4, C3-C4-C5 are smaller than typical hexagonal angle of 120°. This is because of the effect of substitution of $O–CH_3$ groups attached to the C6 of the benzene ring for DMA. The variation in torsional angles C1–C6–O18–C19 = 92.51° (HF), 118.01° (B3LYP) is due to charge delocalization for DMA. The calculated geometric parameters can be used as foundation to calculate the other parameters for the molecule.

5 Vibrational Spectra

Detailed description of vibrational modes can be given by means of normal coordinate analysis. For this purpose, the full set of 75 standard internal coordinates (containing 15 redundancies) for DMA are presented in Table 2. From these, a non-redundant set of local symmetry coordinates is constructed by suitable linear combinations of internal coordinates following the recommendations of Fogarasi *et al.* and they are summarized in Table 3 for DMA. The detailed vibrational assignment of fundamental modes of DMA along with the calculated IR, Raman frequencies and normal mode descriptions (characterized by TED) are reported in Table 4. For visual comparison, the observed and calculated FTIR and FT-Raman spectra of DMA at HF and B3LYP levels using 6-311++G(d,p) basis set are shown in Figs 3 and 4. The vibrational analysis obtained for DMA with the unscaled HF and B3LYP/6-311++G(d,p) force field is generally somewhat greater than the experimental values due to neglect of anharmonicity in real system. These discrepancies can be corrected either by computing anharmonic corrections explicitly or by introducing a scaled field or directly scaling the calculated wave numbers with proper factor[23]. A tentative assignment is often made on the basis of the unscaled frequencies by assuming the observed frequencies so that they are in the same order as the calculated ones. Then, for an easier comparison to the observed values, the calculated frequencies are scaled by the scale to less than 1, to minimize the overall deviation. The results indicate that the B3LYP calculations approximate the observed fundamental frequencies much better than the HF results. Inclusion of electron correlation in density functional theory to a certain extent makes the frequency values smaller in comparison with HF frequency. Also, it should be noted that the experimental results belong to solid phase and theoretical calculations belong to gaseous phase. A better agreement between the computed and experimental frequencies can be obtained by using different scale factors for different regions of vibrations. For that purpose, we have utilized different scaling factors for all fundamental modes except the torsional mode to obtain the scaled frequencies of the compound. The resultant scaled frequencies are also listed in Table 4.

a) C–H vibrations: The hetero aromatic structure shows the presence of C–H stretching vibration in the region 3100 – 3000 cm^{-1} which is the characteristic region for the identification of such C–H stretching vibrations. These vibrations are not found to be affected due to the nature and position of the substituents. In the present investigation, the C–H vibrations are observed at 2998 cm^{-1} in the FTIR spectrum and at 3050, 2920 cm^{-1} in the FT-Raman spectrum, respectively, for DMA and the corresponding force constant contribute to the TED for DMA. The C-H in-plane-bending vibrations usually occur in the region 1390 - 990 cm^{-1} and are very useful for characterization purposes. The C–H out-of-plane bending vibrations occur in the region 900 - 675 cm^{-1} and these bands are highly informative[22]. Accordingly, the IR bands observed at 1038, 994 cm^{-1} and 1000 cm^{-1} in Raman spectrum for DMA have been assigned to, C–H in-plane-bending vibrations. The C–H out-of-plane mode is observed at

Table 2 — Definition of internal coordinates of 3,4-dimethylanisole.

No. (i)	Symbol	Type	Definition[a]
Stretching			
1-3	r_i	CH	C1-H7, C2-H8, C5-H17
4-12	η_i	CH_3(methyl)	C9-H10, C9-H11, C9-H12, C13-H14, C13-H15, C13-H16, C19-H20, C19-H21, C19-H22
13-14	R_i	CO	C6-O7, C19-O18
15-22	q_i	CC	C1-C2,C2-C3,C3-C4,C4-C5,C5-C6,C6-C1, C3-C9,C4-C13
In-plane bending			
23-28	α_i	Ring	C1-C2-C3, C2-C3-C4, C3-C4-C5, C4-C5-C6, C5-C6-C1,C6-C1-C2
29-34	β_i	CCH	C6-C1-H7, C2-C1-H7, C1-C2-H8, C3-C2-H8, C4-C5-H12, C6-C5-H17
35-38	π_i	CCC	C3-C4-C13, C5-C4-C13, C2-C3-C9, C4-C3-C9
39-40	θ_i	CCO	C1-C6-O18, C5-C6-O18
41	θ_i	COC	C6-O18-C19
42-44	υ_i	CCH(methyl)	C4-C13-H14, C4-C13-H15, C4-C13-H16
45-47	β_i	HCH	H11-C9-H10, H12-C9-H10, H11-C9-H12
48-50	υ_i	CCH	C3-C9-H10, C3-C9-H11, C3-C9-H12
51-53	β_i	HCH	H15-C13-H14, H15-C13-H116, H16-C13-H14
54-56	υ_i	OCH	O18-C19-H20, O18-C19-H21, O18-C19-H22
57-59	β_i	HCH	H20-C19-H22, H21-C19-H22, H20-C19-H21
Out-of-plane bending			
60-62	ω_i	CH	H7-C1-C2-C6, H8-C2-C3-C1, H17-C5-C6-C4
63	ψ_i	OC	O18-C6-C5-C1
64	λ_i	CO	C19-O18-C6-(C5,C1)
65-66	δ_i	CC	C9-C3-C2-C4, C13-C4-C5-C3
Torsion			
67-72	τ_i	tRing	C1-C2-C3-C4, C2-C3-C4-C5, C3-C4-C5-C6, C4-C5-C6-C1, C5-C6-C1-C2, C6-C1-C2-C3
73,74	τ_i	tC-CH_3	(C2-C4)-C3-C9-(H10,H11,H12)
75	τ_i	tO-CH_3	C6-O18C19-(H20,H21,H22)

[a] For numbering of atoms refer Fig.1.

869, 830, 754 cm^{-1} in IR for DMA. The observed C–H out-of-plane bending modes show consistent agreement with the computed B3LYP and HF results.

b) C–C vibrations: The C–C hetero aromatic stretching vibrations generally occur in the region[22] 1650 - 1400 cm^{-1}. With heavy substituents, the bonds tend to shift to somewhat lower wavenumbers and greater the number of substituents on the ring, broader the absorption regions. As predicted in the earlier references, the C–C stretching vibrations observed in the present investigation at 1671, 1663, 1650, 1616, 1600, 1597, 1545, 1494 cm^{-1} in FTIR and 1601 cm^{-1} in FT-Raman for DMA. These are assigned for C–C stretching vibrations which are confirmed by their TED values. Most of the ring vibrational modes are affected by the substitutions in the hetero aromatic ring of DMA. The bands observed at 678 cm^{-1} in the FTIR and in Raman 647 cm^{-1} for DMA have been designated to ring in-plane bending modes by careful consideration of their quantitative descriptions. The ring out-of-plane bending modes of DMA are also listed in Table 4.

c) C–O vibrations: The interaction of the carbonyl group with a hydrogen donor group does not produce drastic and characteristic changes in the frequency of the C=O stretch as does by O–H stretch. A great deal of structural information can be derived from the exact position of the carbonyl stretching

Table 3 — Definition of local symmetry coordinates of 3,4-dimethylanisole.

No.	Type	Definition[a]
1-3	CH	r_1, r_2, r_3
4-6	CH_3ss	$\eta_4 + \eta_5 + \eta_6 / \sqrt{3}$, $\eta_7 + \eta_8 + \eta_9 / \sqrt{3}$, $\eta_{10} + \eta_{11} + \eta_{12} / \sqrt{3}$
7-9	CH_3ips	$2\eta_4 + \eta_5 + \eta_6 / \sqrt{6}$, $2\eta_7 + \eta_8 + \eta_9 / \sqrt{6}$, $2\eta_{10} + \eta_{11} + \eta_{12} / \sqrt{6}$
10-12	CH_3ops	$\eta_5 - \eta_6 / \sqrt{6}$, $\eta_8 - \eta_9 / \sqrt{6}$, $\eta_{11} - \eta_{12} / \sqrt{6}$
13,14	CO	R_{13}, R_{14}
15-22	CC	q_{15}, q_{16}, q_{17}, q_{18}, q_{19}, q_{20}, q_{21}, q_{22}
23	Rtrigd	$(\alpha_{23} - \alpha_{24} + \alpha_{25} - \alpha_{26} + \alpha_{27} - \alpha_{28}) / \sqrt{6}$
24	Rsymd	$(-\alpha_{23} - \alpha_{24} + 2\alpha_{25} - \alpha_{26} - \alpha_{27} + 2\alpha_{28}) / \sqrt{12}$
25	Rasymd	$(\alpha_{23} - \alpha_{24} + \alpha_{26} - \alpha_{27}) / \sqrt{2}$
26-28	bCH	$\beta_{29} - \beta_{30} / \sqrt{2}$, $\beta_{31} - \beta_{32} / \sqrt{2}$ $\beta_{33} - \beta_{34} / \sqrt{2}$
29,30	bCC	$\pi_{35} - \pi_{36} / \sqrt{2}$, $\pi_{37} - \pi_{38} / \sqrt{2}$
31	bCO	$\theta_{41} - \theta_{42} / \sqrt{2}$
32	bOC	θ_{43}
33-35	CH_3 sb	$(-\upsilon_{42} - \upsilon_{43} - \upsilon_{44} + \beta_{45} + \beta_{46} + \beta_{47}) / \sqrt{2}$, $(-\upsilon_{48} - \upsilon_{49} - \upsilon_{50} + \beta_{51} + \beta_{52} + \beta_{53}) / \sqrt{2}$, $(-\upsilon_{54} - \upsilon_{55} - \upsilon_{56} + \beta_{57} + \beta_{58} + \beta_{59}) / \sqrt{2}$
36-38	CH_3 ipb	$(2\beta_{45} - \beta_{46} - \beta_{47}) / \sqrt{6}$, $(2\beta_{51} - \beta_{52} - \beta_{53}) / \sqrt{6}$, $(2\beta_{57} - \beta_{58} - \beta_{59}) / \sqrt{6}$
39-41	CH_3 opb	$(\beta_{45} - \beta_{46} / \sqrt{6}$, $(\beta_{51} - \beta_{52} / \sqrt{6}$, $(\beta_{57} - \beta_{58}) / \sqrt{6}$
42-44	CH_3 ipr	$(\upsilon_{42} - \upsilon_{43} + 2\upsilon_{44}) / \sqrt{6}$, $(\upsilon_{48} - \upsilon_{49} + 2\upsilon_{50}) / \sqrt{6}$, $(\upsilon_{54} - \upsilon_{55} + 2\upsilon_{56}) / \sqrt{6}$
45-47	CH_3 opr	$(\upsilon_{43} - \upsilon_{44}) / \sqrt{2}$, $(\upsilon_{49} - \upsilon_{50}) / \sqrt{2}$, $(\upsilon_{55} - \upsilon_{56}) / \sqrt{2}$
48-50	ωCH	ω_{60}, ω_{61}, ω_{63}
51	ψ CO	ψ_{63}
52	λ OC	λ_{64}
53,54	δ CC	δ_{65}, δ_{66}
55	tRtrigd	$(\tau_{67} - \tau_{68} + \tau_{69} - \tau_{70} + \tau_{71} - \tau_{72}) / \sqrt{6}$
56	tRsymd	$(\tau_{67} - \tau_{69} + \tau_{71} - \tau_{72}) / \sqrt{2}$
57	tRasymd	$(-\tau_{67} + 2\tau_{68} - \tau_{69} - \tau_{70} + 2\tau_{71} - \tau_{72}) / \sqrt{12}$
58,59	tCH_3	τ_{73}, τ_{74}
60	$tOCH_3$	τ_{75}

[a] The internal coordinates used here are defined in Table 2.

absorption peak. Susi and Ard[22] identified the C=O stretching mode at 1645 and 1614 cm^{-1}. On referring to the above findings and on the basis of the results of the normal coordinate analysis, the present investigation, the C–O stretching vibrations have been found at 1325 cm^{-1} in IR and 1333, 1326 cm^{-1} in Raman for DMA. These are assigned for C–O stretching vibrations which are confirmed by their TED values. The C–O in-plane and out-of-plane bending vibrations level also have been identified and presented in Table 4 respectively for DMA.

Table 4 — The observed (FTIR and FT-Raman) and calculated (unscaled and scaled) fundamental harmonic frequencies (cm^{-1}), force constant (mdyn A^{-}), infrared - intensity (km/mol), Raman activity (Å amu^{-1}) and probable assignments of 3,4-dimethylanisole are analysed based on SQM force field calculation using HF/6-311++G(d,p) and B3LYP/6-311++G(d,p) method and basis set calculations.

Observed frequencies		HF/6-311++G(d,p)					B3LYP/6-311++G(d,p)					Assignments (TED %)
FTIR	FT-Raman	Unscaled	Scaled	Force Const	IR intensity	Raman activity	Unscaled	Scaled	Force Const	IR intensity	Raman activity	
-	3050ms	3367	3298	7.3204	13.0182	131.067	3198	3055	6.5920	9.7133	140.369	υCH(99)
2998ms	-	3353	3284	7.2397	11.4032	83.4071	3184	3004	6.5131	13.9258	64.2420	υCH(98)
-	2920vw	3339	3265	7.1632	19.7124	65.2254	3155	2928	6.3917	24.9726	89.3201	υCH(97)
2944s	-	3294	3254	7.0483	52.6631	141.110	3140	2946	6.3815	24.2933	127.624	CH3ss(81), υCH(19)
2919ms	-	3265	3210	6.9195	17.0604	86.1532	3091	2920	6.1780	9.3308	94.7180	CH3ss(75), υCH(22)
-	2911vw	3260	3188	6.8968	40.2546	34.0394	3088	2914	6.1650	43.2780	17.2558	CH3ss(74), υCH(26)
-	2900vw	3239	3161	6.8405	44.6059	37.7461	3066	2909	6.1220	46.1665	57.8081	CH3ips(70), CH3ops(29)
-	2868vw	3232	3152	6.7834	35.7924	100.052	3052	2874	6.0263	17.1368	60.0205	CH3ips(72), CH3ops(28)
2862ms	-	3227	3144	6.7643	17.7954	46.5883	3044	2867	5.9964	34.8103	111.666	CH3ips(71), CH3ops(22)
2732vw	-	3182	3104	6.1924	60.6823	303.947	3004	2736	5.5159	45.4562	265.563	CH3ops(69), CH3ips(23)
2747vw	-	3179	3078	6.1768	13.9553	85.4549	2999	2735	5.4963	22.2468	337.240	CH3ops(80), CH3ips(20)
1688s	-	3177	3059	6.1485	71.4907	42.9794	2998	1692	5.4789	77.6894	26.4364	CH3ops(78), CH3ips(21)
1671vs	-	2810	2804	11.361	53.1519	27.9519	2644	1678	8.5212	60.4322	43.6898	υCC(66), CH3ipb(23)
1663vs	-	2765	2761	11.690	26.1635	13.2360	2618	1670	9.3978	16.1396	13.0362	υCC(62), CH3ipb(27)
1650s	-	2671	2632	4.2744	94.2255	2.2970	2516	1655	2.2835	52.2458	8.0040	υCC(60), CH3ipb(30)
1616s	-	2633	2610	1.6591	12.1127	8.5839	2535	1619	1.4509	22.3845	9.5139	υCC(61), CH3sb(32)
1600vs	1601vw	2621	2601	1.6866	13.7312	1.8316	2534	1608	1.4766	36.9079	6.1869	υCC(63), CH3sb(36)
1597ms	-	2620	2589	1.6615	2.3117	18.144	2529	1600	1.5632	34.7906	4.8882	υCC(62), CH3sb(27)
1545w	-	2618	2562	1.6146	15.318	5.7808	2524	1549	1.8546	23.0857	4.5959	υCC(61), υCO(23)
1494s	-	2613	2544	1.8112	6.6660	1.7982	2522	1499	1.4371	12.1876	13.844	υCC(70), υCO(28)
1469vs	-	2607	2534	1.7982	11.495	3.1874	2519	1475	1.4265	0.3769	21.358	CH3ipb(79), υCC(20)
-	1452w	1803	1790	1.5832	0.0105	15.283	1687	1459	1.5388	1.3981	5.5779	CH3ipb(78), υCC(22)
-	1398w	1657	1598	3.2775	11.793	0.3605	1559	1405	1.5278	10.092	28.925	CH3ipb(77), υCC(21)
1383vs	-	1634	1589	1.7537	0.3784	13.192	1549	1389	1.5068	3.2971	12.126	CH3sb(66), υCC(31)
1377vs	-	1598	1496	1.9671	2.4865	4.6810	1472	1386	3.5404	3.6515	2.3014	CH3sb(65), υCC(32)
1364vs	-	1522	1400	2.2572	94.519	9.7863	1374	1370	2.6092	26.266	7.5410	CH3sb(73), υCC(27)
-	1333vw	1396	1388	2.7402	86.7268	15.805	1361	1338	2.3728	0.6263	3.0666	υCO(70), υCC(22)
1325vs	1326vw	1386	1370	1.8273	5.8370	6.5708	1356	1334	5.1142	92.448	31.661	υCO(72), υCC(27)
-	1305w	1379	1356	1.7737	23.788	0.7980	1323	1314	2.3080	66.837	1.8460	CH3opr(71),CH3opb(23)
1291vs		1361	1340	2.3837	2.2649	2.4023	1334	1298	1.4151	27.067	2.2806	CH3opr(70),CH3opb(28)
1265s	1265w	1356	1312	1.2248	4.2241	2.7888	1292	1278	1.1790	8.7350	3.6997	CH3opr(69), CH3opb(21)
1191s		1310	1299	3.2248	40.877	5.6505	1256	1199	0.9883	0.4411	5.3683	CH3opb(68), CH3ips(20)
1180vs	-	1288	1278	1.4138	6.8264	3.7899	1272	1188	1.4198	23.883	7.0442	CH3opb(60), CH3ips(32)
1162s	-	1270	1258	1.2963	0.0231	0.0711	1209	1172	1.0980	0.0200	0.1537	CH3opb(66), CH3ips(30)
1151ms	1150w	1259	1221	2.8960	90.503	7.7754	1172	1159	0.9600	5.7256	0.6792	Rasym(61), bCH(22)
1090s	-	1246	1109	1.1206	1.2851	0.1251	1148	1109	1.2252	52.553	0.2649	Rsymd(64), bCH(20)
1072vs	-	1199	1160	1.1596	2.8342	0.8635	1130	1080	1.0350	2.6303	1.4172	Rtrigd(63), bCH(32)
1038w	-	1099	1081	1.1218	9.6434	1.2322	1064	1048	1.6534	28.201	5.2977	bCH(56), Rasym(35)
-	1000vs	1071	1051	0.9190	0.1928	0.0793	1031	1010	0.7240	0.0127	0.0724	bCH(51), Rsymd(44)
994vw	-	1066	1045	1.9829	13.355	11.931	1029	1005	2.3866	7.0238	9.3966	bCH(60), Rtrigd(25)
974w	-	1045	1034	0.8909	9.4264	1.4299	998	983	0.6399	20.109	0.0491	CH3ipr(59), ωCH(36)
961ms	-	1023	1007	0.7141	24.966	1.0417	987	973	0.5721	41.413	0.1003	CH3ipr(50), ωCH(46)
953ms	-	1018	999	1.6377	0.0231	26.856	863	965	1.5568	0.5228	25.967	CH3ipr(57), ωCH(38)
869vs	-	1000	856	1.0378	6.4098	2.8274	878	878	0.9184	1.7254	0.4351	ωCH(51), bCC(33)
830vs	-	989	978	1.5132	5.3736	1.3759	961	844	1.5278	9.7656	2.1709	ωCH(55), bCC(43)

(*Contd.*)

Table 4 — The observed (FTIR and FT-Raman) and calculated (unscaled and scaled) fundamental harmonic frequencies (cm^{-1}), force constant (mdyn A^{-}), infrared - intensity (km/mol), Raman activity (Å amu^{-1}) and probable assignments of 3,4-dimethylanisole are analysed based on SQM force field calculation using HF/6-311++G(d,p) and B3LYP/6-311++G(d,p) method and basis set calculations. (*Contd*.)

Observed frequencies		HF/6-311++G(d,p)					B3LYP/6-311++G(d,p)					Assignments (TED %)
FTIR	FT-Raman	Unscaled	Scaled	Force Const	IR intensity	Raman activity	Unscaled	Scaled	Force Const	IR intensity	Raman activity	
754s	-	967	657	0.8553	7.5135	0.9489	927	763	0.6505	1.9775	0.2870	ωCH(54), bCO(41)
678w	-	892	861	0.9163	2.5972	10.287	828	687	0.7841	3.9002	8.3260	bCC(53), bCO(32)
-	647ms	867	856	0.6047	5.1692	2.3575	724	655	0.6803	1.7935	2.3161	bCC(52), t Rasym(40)
601ms	601s	708	699	0.4831	2.4621	0.3759	663	619	0.5128	6.2353	6.1291	bCO(51), t Rsymd(49)
-	590ms	688	669	0.5691	7.4146	2.5788	660	601	0.3496	4.4608	0.1473	t Rasym(50), ωCC(46)
-	588w	656	634	0.3929	1.3772	3.7937	612	598	0.2984	1.0550	4.3791	t Rsymd(49), ωCC(43)
-	563w	634	612	0.2672	2.4367	0.2666	601	572	0.2616	6.6160	1.7813	t Rtrigd(48),
-	522ms	599	570	0.1611	0.8795	0.2719	536	532	0.1395	0.3204	0.2761	bCO(47), t Rtrigd(48)
-	491ms	545	534	0.3156	2.2662	2.1947	512	499	0.0508	0.2195	0.9699	ωCC(46), ωCO(38)
482ms		522	514	0.0619	1.5662	1.6748	500	491	0.0748	2.3039	1.5839	ωCC(45), ωCO(34)
478vw		523	512	0.0224	0.5686	0.1613	499	487	0.0374	0.5282	1.6003	ωCO(66)
-	390w	512	501	0.0198	0.4715	0.0968	489	407	0.0213	1.5328	0.4890	ωCO(63)
-	292vw	399	378	0.0099	0.0586	0.1594	358	305	0.0249	0.3995	0.6629	tCH3(72)
-	277w	368	356	0.0244	1.9389	0.8937	315	289	0.0108	0.1676	0.4531	tCH3(70)
-	256vw	345	323	0.0016	4.6974	0.6553	312	268	0.0098	5.8351	0.1763	tCH3(65)

Abbreviations: ν - stretching; b - in-plane bending; ω - out-of-plane bending; asymd - asymmetric; symd - symmetric; t - torsion; trig - trigonal; w - weak; vw - very week; vs - very strong; s - strong; ms - medium strong; ss - symmetric stretching; ass - asymmetric stretching; ips - in-plane stretchingj; ops - out-of-plane stretching; sb - symmetric bending; ipr - in-plane rocking; opr - out-of-plane rocking; opb - out-of-plane bending.

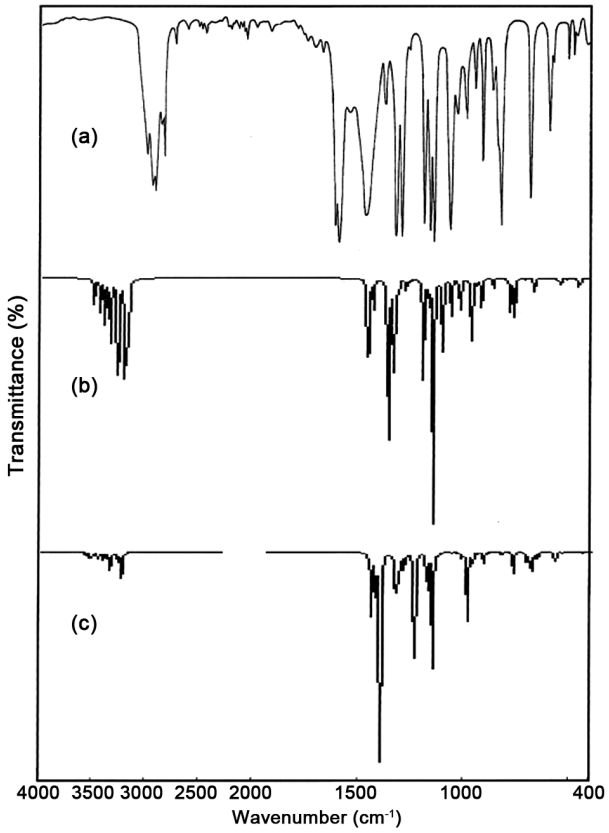

Fig. 3 — Comparison of observed and calculated infrared spectra of 3,4-dimethylanisole (a) observed, (b) HF/6-311++G(d,p) and (c) B3LYP/6-311++G(d,p).

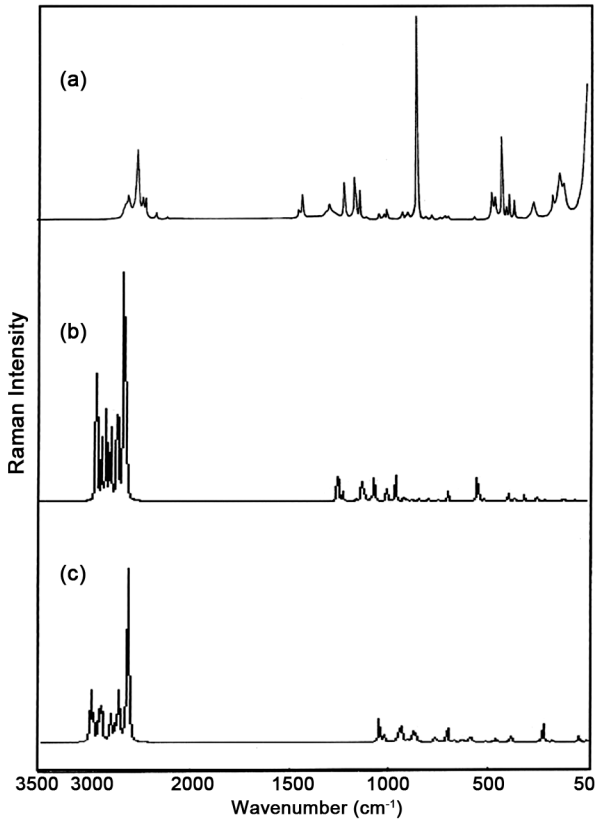

Fig. 4 — Comparison of observed and calculated Raman spectra of 3,4-dimethylanisole (a) observed, (b) HF/6-311++G(d,p) and (c) B3LYP/6-311++G(d,p).

d) CH_3 group vibrations: The investigated molecule under consideration possesses CH_3 groups in third, fourth position of DMA. For the assignments of CH_3 group frequencies one can expected that nine fundamentals can be associated to each CH_3 group, namely three stretching, three bending, two rocking modes and a single torsional mode describe the motion of methyl group. The CH_3 symmetric stretching frequency is identified at 2944, 2919 cm^{-1} in the FTIR spectrum and 2911 cm^{-1} in the FT-Raman spectrum for DMA. The CH_3 in-plane stretching vibrations are identified at 2862 cm^{-1} in the FTIR spectrum and 2900, 2868 cm^{-1} in the FT-Raman spectrum for DMA. The CH_3 symmetric bending and CH_3 in-plane bending frequencies are attributed at 1383, 1377, 1364 cm^{-1} and 1469 cm^{-1} in the FTIR spectrum and 1452, 1398 cm^{-1} in the FT Raman spectrum for DMA. These assignments are supported by literature[22]. The in-plane rocking and out-of-plane rocking modes of CH_3 group are found at 974, 961, 953 cm^{-1} and 1291, 1265 cm^{-1} in the FTIR spectrum and 1305, 1265 cm^{-1} in the FT-Raman spectrum for DMA. The bands obtained at 2732, 2747, 1688 cm^{-1} and 1191, 1180, 1162 cm^{-1} in the FTIR spectrum for DMA assigned to CH_3 out-of-plane stretching and CH_3 out-of-plane bending modes, respectively. The assignment of the bands at 292, 277, 256 cm^{-1} in the FT Raman spectrum for DMA attributed to methyl twisting mode.

e) The thermodynamic parameters namely heat capacity, entropy, rotational constants, dipole moments, vibrational and zero-point vibrational energies of the compound have also been computed at *ab initio* HF and DFT/B3LYP levels using 6-311++G(d,p) as basis set and are presented in Table 5 for DMA. The difference in the values calculated by both the methods is marginal. The variation in the ZPVE seems to be insignificant. The ZPVE is much lower by the DFT/B3LYP method than by the HF method. The total energy and the change in the total entropy of the molecule at room temperature are also presented. Dipole moment reflects the molecular charge distribution and is given as a vector in three dimensions. Therefore, it can be used as descriptor to depict the charge movement across the molecule. Direction of the dipole moment vector in a molecule depends on the centers of positive and negative charges. Dipole moments are strictly determined for neutral molecules. For charged systems, its value depends on the choice of origin and molecular orientation. As a result of HF and DFT (B3LYP) calculations, the highest dipole moment is observed for B3LYP/6-311++G(d,p) level whereas the lowest one is observed for HF/6-311++G(d,p) level in the molecule. The total dipole moment of DMA determined by HF and B3LYP level using 6-311++G(d,p) basis set is 0.6669, 0.7351 Debye, respectively.

6 Prediction of First Hyperpolarizability

The first hyperpolarizability (β_0) of this novel molecular system and the related properties (β_0, α_0) of DMA are calculated using the B3LYP/ 6-311++G(d,p) basis set, based on the finite field approach. In the presence of an applied electric field, the energy of a system is a function of the electric field. The first hyperpolarizability is a third-rank tensor that can be described by a $3 \times 3 \times 3$ matrix. The 27 components of the 3D matrix can be reduced to 10

Table 5 — The thermodynamic parameters of 3,4-dimethylanisole calculated at HF/6-311++G(d,p) with B3LYP/6-311+G(d,p) and 6-311++G(d,p) method and basis set calculations.

Parameters	HF/ 6-311++G(d,p)	B3LYP/ 6-311++G(d,p)
Optimized global minimum Energy (Hartrees)	–422.6826	–425.3990
Total energy(thermal), E_{total} (kcal mol^{-1})	131.847	124.465
Translational	0.889	0.889
Rotational	0.889	0.889
Vibrational	130.070	122.687
Molar capacity at constant volume (cal mol^{-1} k^{-1})		
Total	35.916	38.243
Translational	2.981	2.981
Rotational	2.981	2.981
Vibrational	29.954	32.281
Entropy		
Total	98.138	97.513
Translational	40.637	40.637
Rotational	29.644	29.716
Vibrational	27.857	27.161
Zero point vibrational energy (Kcal mol^{-1})	125.6337	118.0599
Rotational constants(GHZ)		
A	2.7041	2.5989
B	0.8820	0.8902
C	0.6998	0.6714
Rotational temperature (Kelvin)	0.12978 0.04233 0.0335	0.1247 0.0427 0.0322

components due to the Kleinman symmetry [23]. It can be given in the lower tetrahedral. The components of β are defined as the coefficients in the Taylor series expansion of the energy in the external electric field. When the external electric field is weak and homogenous, this expansion becomes:

$$E = E_0 - \mu_\alpha F_\alpha - \frac{1}{2}\alpha_{\alpha\beta}F_\alpha F_\beta - \frac{1}{6}\beta_\alpha\beta_\gamma F_\alpha F_\beta F_\gamma + ...$$

where E_0 is the energy of the unperturbed molecules, F_α the field at the origin and μ_α, $\alpha_{\alpha\beta}$ and $\beta_\alpha\beta_\gamma$ are the components of dipole moment, polarizability and the first hyperpolarizabilities, respectively. The total static dipole moment μ, the mean polarizability α_0 and the mean first hyperpolarizability β_0, using the *x*, *y*, *z* components they are defined as:

$$\mu = \left(\mu_x^2 + \mu_y^2 + \mu_z^2\right)^{1/2}$$

$$\alpha_0 = \frac{\left(\alpha_{xx} + \alpha_{yy} + \alpha_{zz}\right)}{3}$$

$$\alpha = 2^{-1/2}\left[\left(\alpha_{xx} - \alpha_{yy}\right)^2 + \left(\alpha_{yy} - \alpha_{zz}\right)^2 + \left(\alpha_{zz} - \alpha_{xx}\right)^2 + 6\alpha_{xx}^2\right]^{1/2}$$

$$\beta_0 = \left(\beta_x^2 + \beta_y^2 + \beta_z^2\right)^{1/2}$$

$$\beta_{vec} = \frac{3}{5\left[\left(\beta_x^2 + \beta_y^2 + \beta_z^2\right)^{1/2}\right]}$$

where

$$\beta_x = \beta_{xxx} + \beta_{xyy} + \beta_{xzz}$$

$$\beta_y = \beta_{yyy} + \beta_{yxx} + \beta_{yzz}$$

$$\beta_z = \beta_{zzz} + \beta_{zxx} + \beta_{zyy}$$

The β_0 components of GAUSSIAN 09W output are reported in atomic units and therefore the calculated values are converted into e.s.u. units (1 a.u. = 8.3693×10^{-33} e.s.u.). The calculated value of hyperpolarizability and polarizability of DMA are given in Table 6. The title molecules are an attractive object for future studies of non-linear optical properties.

7 HOMO-LUMO Band Gap

This electronic absorption corresponds to the transition from the ground to the first excited state and is mainly described by one electron excitation from the highest occupied molecular orbital (HOMO) to the lowest unoccupied molecular orbital (LUMO)[23]. Many organic molecules, containing conjugated π electrons are characterized by large values of molecular first hyper polarizabilities and analyzed by means of vibrational spectroscopy. In most of the cases, even in the absence of inversion symmetry, the band in the Raman spectrum is weak in the IR spectrum and vice-versa. But the intra molecular charge from the donor to acceptor group through a single-double bond conjugated path can induce large variations of both the molecular dipole moment and the molecular polarizability, making IR and Raman activity strong at the same time. The analysis of the wave function indicates that the electron absorption corresponds to the transition from the ground to the first excited state and is mainly described by one-electron excitation from the highest occupied molecular orbital (HOMO) to the lowest unoccupied orbital (LUMO). In DMA, the HOMO is located over heterocyclic ring and the HOMO-LUMO transition implies an electron density transfer to the CH_3 group from heterocyclic ring and oxygen atom, whereas in DMA the HOMO is located over benzene ring, especially on oxygen atom, and the HOMO-LUMO transition implies an electron density transfer to the heterocyclic ring from CH_3 atom. Moreover, the composition of HOMO and LUMO for DMA is shown in Fig. 5. The HOMO-LUMO energy gap of DMA are calculated at B3LYP/6-311++G(d,p) level, which reveals that the energy gap reflects the

Table 6 — Nonlinear optical properties of 3,4-dimethylanisole and 3-methyl-2-nitroanisole calculated at HF/6-311++G(d,p) with B3LYP/6-311+G(d,p) and 6-311++G(d,p) method and basis set calculations.

NLO behaviour	DMA	
	HF/6-311++G(d,p)	B3LYP/6-311++G(d,p)
Dipole moment(μ)	0.6669Debye	0.7351Debye
Mean polarizability (α)	0.8664×10^{-30} esu	0.9388×10^{-30} esu
Anisotropy of the polarizabilty (Δ_α)	1.9482×10^{-30} esu	2.6070×10^{-30} esu
First hyperpolarizability (β)	0.6947×10^{-30} esu	2.4708×10^{-30} esu
Vector – first hyperpolarizability (β_{vec})	0.4168×10^{-30} esu	1.4825×10^{-30} esu

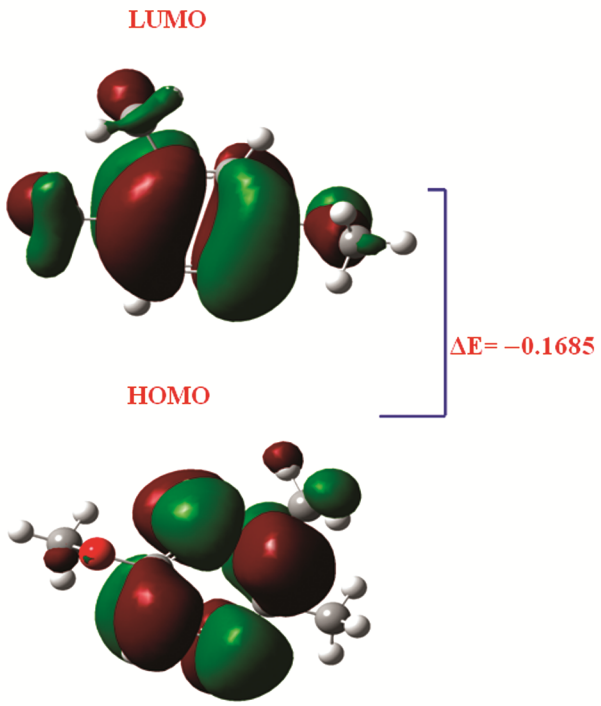

Fig. 5 — HOMO-LUMO plot of 3,4-dimethylanisole.

chemical activity of the molecules. The LUMO as an electron acceptor (EA) represents the ability to obtain an electron (ED) and HOMO represents ability to donate an electron (ED). The ED groups to the efficient EA groups through π -conjugated path. The strong charge transfer interaction through π-conjugated bridge results in substantial ground state donor-acceptor (DA) mixing and the appearance of a charge transfer band in the electron absorption spectrum. The HOMO and LUMO energy gap explains the fact that eventual charge transfer interaction is taking place within the title molecules.

Based on density functional descriptors global chemical reactivity descriptors of compounds such as hardness, chemical potential, softness, electronegativity and electrophilicity index as well as local reactivity have been defined[24]. Pauling introduced the concept of electronegativity as the power of an atom in a compound to attract electrons to it. Hardness (η), chemical potential (μ) and electronegativity (χ) and softness are defined follows:

$$\eta = \frac{1}{2}\left(\partial^2 E/\partial N^2\right)_{V(r)} = \frac{1}{2}\left(\partial\mu/\partial N\right)_{V(r)}$$

$$\mu = \left(\partial E/\partial N\right)_{V(r)}$$

$$\chi = -\mu = -\left(\partial E/\partial N\right)_{V(r)}$$

where E and $V(r)$ are electronic energy and external potential of an N-electron system, respectively. Softness is a property of compound that measures the extent of chemical reactivity. It is the reciprocal of hardness.

$$S = \frac{1}{\eta}$$

Using Koopman's theorem for closed-shell compounds, η, μ and χ can be defined as:

$$\eta = \frac{\left(I - A\right)}{2}$$

$$\mu = \frac{-\left(I + A\right)}{2}$$

$$\chi = \frac{\left(I + A\right)}{2}$$

where A and I are the ionization potential and electron affinity of the compounds, respectively. Electron affinity refers to the capability of a ligand to accept precisely one electron from a donor. However in many kinds of bonding viz. covalent hydrogen bonding, partial charge transfer takes places. Recently Parr *et al.*[25] have defined a new descriptor to quantity the global electrophilic power of the compound as electrophilicity index (ω), which defines a quantitative classification of the global electrophilic nature of a compound have proposed electrophilicity index (ω) as a measure of energy lowering due to maximal electron flow between donor and acceptor. They defined electrophilicity index (ω) as follows:

$$\omega = \mu^2/2\eta$$

The usefulness of this new reactivity quantity has been recently demonstrated in understanding the toxicity of various pollutants in terms of their reactivity and site selectivity. The calculated value of electrophilicity index describes the biological activity for DMA, respectively. All the calculated values of HOMO-LUMO, energy gap, ionization potential, Electron affinity, hardness, potential, softness and electrophilicity index are given in Table 7.

8 NBO Analysis

The NBO analysis is carried out by examining all possible interactions between 'filled' (donor) Lewis-type NBOs and 'empty' (acceptor) non-Lewis NBOs, and estimating their energetic important by 2nd order perturbation theory. Since these interactions lead to loss of occupancy from the localized NBOs of the

Table 7 — HOMO-LUMO energy gap and related molecular properties of 3,4-dimethylanisole and 3-methyl-2-nitroanisole.

Molecular Properties	DMA
	B3LYP/6-311++G(d,p)
HOMO	–0.3119
LUMO	–0.1434
Energy gap	–0.1685
Ionisation Potential (I)	0.3119
Electron affinity(A)	0.1434
Global softness(s)	11.8687
Global Hardness (η□)	0.0842
Chemical potential (μ)	–0.2276
Global Electrophilicity (ω)	–0.3076

idealized Lewis structure into the empty non-Lewis orbitals, they are referred to as delocalization corrections to the zeroth-order natural Lewis structure. For each donor NBO (i) and acceptor NBO (j) with delocalization $i \rightarrow j$ is estimated as:

$$E^{(2)} = \Delta E_{ij} = q_i \frac{F(i,j)^2}{\varepsilon_j - \varepsilon_i}$$

where q_i is the donor orbital occupancy ε_j and ε_i are diagonal elements orbital energies and $F(i, j)$ is the off diagonal NBO Fock matrix element. The larger $E^{(2)}$ value, the more intensive is the interaction between electron donors and acceptors, *i.e.*, the more donation tendency from electron donors to electron acceptors and the greater the extent of conjugation of the whole system. DFT (B3LYP/6-311++G(d,p)) level computation is used to investigate the various second-order interactions between the filled orbitals of one subsystem and vacant orbitals of another subsystem, which is a measure of the delocalization or hyper-conjugation[26]. NBOs are localized electron pair orbitals for bonding pairs and lone pairs. The hybridization of the atoms and the weight of each atom in each localized electron pair bond are calculated in the idealized Lewis structure. A normal Lewis structure would not leave any antibonding orbitals, so the presence of antibonding orbitals shows deviations from normal Lewis structures. Anti bonding localized orbitals are called non-Lewis NBOs. In order to study the small deviations from idealized Lewis structure, the donor–acceptor interaction approach is adopted. In DMA, π(C3–C4)→π*(C1–C2), interaction is seen to give a strong stabilization 45.18 kJ/mol. This strong stabilization denotes the larger delocalization. The interesting interactions in DMA molecule are LP1O18, LP2O18 with that of antibonding C5–C6, C1–C6. These two interactions result the stabilization energy of 8.870, 12.59 kJ/mol, respectively. This highest interaction around the ring can induce the large bioactivity in the molecule. This shows that the lone pair orbital participates in electron donation in the molecule. The calculated values of $E^{(2)}$ are shown in Table 8 for DMA, respectively.

9 ^{13}C and ^{1}H NMR Spectral Analysis

The molecular structure of DMA and MNA is optimized by using B3LYP method with 6-31++G basis set. Then, GIAO ^{13}C calculations of the title compound are calculated and compared with experimental values[27] which are shown in Table 9. Relative chemical shifts are then estimated by using the corresponding TMS shielding calculated in advance at the theoretical level as reference. Changes in energy needed to flip protons are called chemical shifts. The location of chemical shifts (peaks) on a NMR spectrum is measured from a reference point that the hydrogen in a standard reference compound –$(CH_3)_4Si$ or tetramethylsilane (TMS)– produce. The amount of energy necessary to flip protons in TMS is assigned the arbitrary value of zero δ. Chemical shifts are measured in parts per million magnetic field strength difference (δ-scale), relative to TMS. The experimental values of DMA for ^{1}H and ^{13}C isotropic chemical shielding for TMS are 31.94, 34.76 ppm, respectively[28]. All the calculations are performed using Gauss view molecular visualization program and GAUSSIAN 09W program package. The result shows that the range ^{13}C NMR chemical shift of the typical organic compound usually is > 100 ppm, the accuracy ensures reliable interpretation of spectroscopic parameters. It is true from the above literature value in our present study, that the title compound also shows the same. In practice, it is easier to fix the radio wave frequency and vary the applied magnetic field than it is to vary the radio wave frequency. The magnetic field "felt" by a hydrogen atom is composed of both applied and induced fields. The induced field is a field created by the electrons in the bond to the hydrogen and the electrons in nearby π bonds. When the two fields reinforce each other, a smaller applied field is required to flip the proton. In this situation, a proton is said to be deshielded. When the applied and induced fields oppose each other, a stronger field must be applied to flip the proton. In this state, the proton is

Table 8 — Second-order perturbation theory analysis of Fock matrix in NBO basis of 3,4-dimethylanisole using DFT/B3LYP/6-311++G(d,p) methods and basis set calculations.

Donor (i)	Hybrid (%S)	Type	Occupancy	Acceptor (j)	Type	$E^{(2)a}$ (kJ/mol)	E(j)–E(i)[b] (a.u)	F(i,j)[c] (a.u)
C1-C2	35.98/35.11	σ	0.98635	C3-C9	*σ	8.11696	1.07	0.058
C1-C2		π	0.84085	C6-O18	*σ	9.2048	0.97	0.058
C1-C2		π		C3-C4	*π	41.5471	0.29	0.069
C1-C2		σ		C5-C6	*π	45.229	0.27	0.069
C1-C6	35.64/37.84	σ	0.98964	C5-C6	*σ	7.65672	1.25	0.061
C1-H7	28.36/99.91	σ	0.98856	C2-C3	*σ	8.03328	1.08	0.058
C2-C3	36.40/34.79	σ	0.98695	C3-C4	*σ	9.24664	1.27	0.067
C2-H8	28.45/99.93	σ	0.98981	C1-C6	*σ	7.82408	1.07	0.057
C3-C4	35.64/35.68	σ	0.98573	C2-C3	*σ	8.40984	1.26	0.064
C3-C4		π	0.81959	C1-C2	*π	45.1872	0.27	0.069
C3-C9	29.54/28.71	σ	0.98919	C4-C5	*σ	7.9496	1.16	0.059
C4-C5	34.61/36.50	σ	0.98459	C3-C4	*σ	9.03744	1.27	0.066
C4-C13	29.68/28.69	σ	0.98909	C2-C3	*σ	7.90776	1.17	0.059
C5-C6	35.19/37.94	σ	0.98870	C1-C6	*σ	7.48936	1.25	0.06
C5-H17	28.28/99.96	σ	0.98852	C1-C6	*σ	8.53536	1.07	0.059
C9-H11	23.43/99.97	σ	0.98956	C3-C4	*π	8.07512	0.55	0.045
C13-H16	23.45/99.97	σ	0.98929	C3-C4	*π	8.24248	0.55	0.046
O18		LP(1)	0.97384	C5-C6	*π	8.87008	0.59	0.048
O18		LP(2)	0.97138	C1-C6	*σ	12.5938	0.84	0.064
O18		LP(2)		C5-C6	*σ	12.6775	0.84	0.064
O18		LP(2)		C19-H20	*σ	11.757	0.7	0.056
C5-C6	0.01/0.05	*π	0.18419	C3-C4	*π	322.837	0.02	0.082

[a] $E^{(2)}$ means energy of hyper conjugative interaction (stabilization energy).
[b] Energy difference between donor and acceptor i and j NBO orbitals.
[c] F (i, j) is the Fork matrix element between i and j NBO orbitals.

Table 9 — The calculated shifts of carbon and hydrogen atoms of 3,4-dimethyl anisole using B3LYP/6-311++G(d,p) GIAO method.

Atom position	Isotropic chemical shielding tensor (σ) (ppm)	Chemical shifts (δ) (ppm)		
		Theoretical	Expt[a]	Δ
1C	96.2875	86.1781	101.4	15.219
2C	87.8080	94.6576	98.94	4.2824
3C	87.5200	94.9456	99.92	4.9744
4C	82.4465	100.019	121.7	21.681
5C	94.4103	88.0553	99.87	11.8147
6C	59.3799	123.089	110.32	12.769
7H	26.6283	27.6432		
8H	26.2159	27.1423		
9C	195.8329	197.833		
10H	31.6410	31.542		
11H	31.8210	31.83		
12H	31.9751	31.9493		
13C	195.2237	195.223		
14H	31.5930	31.593		
15H	31.9493	31.9493		
16H	31.7571	26.5624		
17H	26.5624	26.5624		
18O	316.0591	3.9008	5.809	1.9082
19C	161.3033	161.303	176.67	15.367
20H	30.8845	30.885		
21H	29.9136	29.913		
22H	30.8825	30.885		

[a]Taken from Ref.[28] and $\Delta(\delta_{exp}-\delta_{the})$; difference between respective chemical shifts.

shielded. Electronegative atoms such as CH_3, O and halogens deshield hydrogen. The extent of deshielding is proportional to the electronegativity of the heteroatom and its proximity to the hydrogen. The oxygen atom show electronegative property, so that the chemical shift of C4, C6, C9, C13 and C19 seems to be 100.01, 123.08, 197.83, 195.22 and 161.30 ppm for DMA. The chemical shift of C9 is greater than the other carbon values. This increase in chemical shift is due to the substitution of more electronegative oxygen and nitro atoms in the benzene ring. The presence of electronegative atom attracts all electron clouds of carbon atoms towards the oxygen and nitro atoms, which leads to deshielding of carbon atom and net result in increase in chemical shift value. The NMR shielding surfaces of C9, C2 is shown in this work the chemical shift (δ) for carbon atoms presented in the DMA in gas phase has been studied and theoretical ^{13}C, ^{1}H-NMR isotropic shielding of carbon and hydrogen atom. In the NMR shielding surfaces, the blue region represents shielding and red region represents de-shielding are shown in Fig. 6 for DMA, respectively.

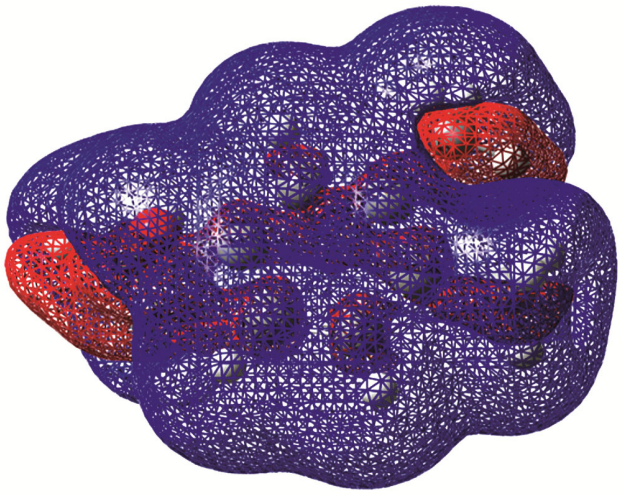

Fig. 6 — NMR shielding surface of 3,4-dimethylanisole.

10 Conclusions

The molecular structural parameters, thermodynamic properties and fundamental vibrational frequencies of the optimized geometry of 3,4-dimethylanisole have been obtained from *ab initio* HF and DFT calculations. The theoretical results are compared with the experimental vibrations. The computed geometrical parameters are in good agreement with the observed X-ray diffraction data of similar compound. Although both types of calculations are useful to explain vibrational spectra of 3,4-dimethylanisole, *ab initio* calculations at HF/6-311++G(d,p) level is found little poorer than DFT-B3LYP/6-311++G(d,p) level calculations. On the basis of agreement between the calculated and experimental results, assignments of all the fundamental vibrational modes of 3,4-dimethylanisole have been made for the first time in this investigation. The TED calculation regarding the normal modes of vibration provides a strong support for the frequency assignment. Therefore, the assignments proposed at higher level of theory with higher basis set with only reasonable deviations from the experimental values seem to be correct. HOMO and LUMO energy gap explains the eventual charge transfer interactions taking place within the molecule. Furthermore, the nonlinear optical, first-order hyperpolarizabilities and total dipole moment properties of the molecule show that the title molecule is an attractive object for future studies of nonlinear optical properties. NMR, NBO analysis have been performed in order to elucidate charge transfers or conjugative interaction, the intra-molecule rehybridization and delocalization of electron density within the molecule.

References

1 Naoki M, Shusuke N, Satoshi T & Takeaki E, *Opt Commun*, 260 (2006) 25.

2 Espin J C, Tudela J & Garcia-Canovas F, *Anal Biochem*, 259 (1998) 118.

3 Gordon J P, Leite R C C, Moore R S, Porte S P S & Whinnery J R, *J Appl Phys*, 36 (1965) 3.

4 Sheldon S J, Knight L V & Thorne J M, *Appl Opt*, 21 (1982) 1663.

5 Jurgensen F & Schroer W, *Appl Opt*, 34 (1995) 41.

6 Frisch M J, Trucks G W & Schlegal H B, GAUSSIAN 09, Revision A02, Gaussian, Inc, Wallingford, CT, 2009.

7 Schlegel H B, *Comput J Chem*, 3 (1982) 214.

8 Becke A D, *Chem J Phys*, 98 (1993) 5648.

9 Lee C, Yang W & Parr R G, *Phys Rev B*, 37 (1988) 785.

10 Pulay P, Fogarasi G, Pongor G, Boggs J E & Vargha A, *Am Chem J Soc*, 105 (1983) 7037.

11 Rauhut G & Pulay P, *Phys J Chem*, 99 (1995) 3093.

12 Fogarasi G & Ulay P, in: Durig J R (Ed) *Vibrational spectra and structure*, (Elsevier: Amsterdam), 14 (1985) 125.

13 Fogarasi G, Zhou X, Taylor P W & Pulay P, *J Am Chem Soc*, 114 (1992) 8191.

14 Sundius T, *J Mol Struct*, 218 (1990) 321.

15 Sundius T, *Vib Spectrosc*, 29 (2002) 89.

16 MOLVIB (V.7.0): *Calculation of harmonic force fields and vibrational modes of molecules*, QCPE Program No- 807 (2002).

17 Frisch A, Nielson A B & Holder A J, Gaussview user manual, Gaussian Inc, Pittsburg, P A, 2000.

18 Polavarapu P L, *J Phys Chem*, 94 (1990) 8106.

19 Keresztury G, *Raman spectroscopy theory*, in: Chalmers J M & Griffiths R (Eds), *Handbook of vibrational spectroscopy*, (John Wiley & Sons Ltd), 1 (2002) 71.

20 Keresztury G, Holly S, Varga J, Besenyei G, Wang A Y & Durig J R, *Spectroschim Acta A*, 49A (1993) 2007.

21 Cheng X W, *Acta Crystallogr*, E63 (2007) 03797.

22 Sambathkumar K, *Density functional theory studies of vibrational spectra, HOMO- LUMO, NBO and NLO analysis of some cyclic and heterocyclic compounds* (Ph.D. Thesis), Bharathidasan University, Tiruchirappalli, August 2014.

23 Sambathkumar K, *Spectrochim Acta A*, 147 (2015) 51.

24 Sambathkumar K, *Elixir Vib Spec*, 91 (2016) 38381.

25 Parr R G, Szentpaly L V & Liu S J, *Am Chem Soc*, 121 (1999) 1922.

26 Sambathkumar K & Nithiyanantham S, *J Mater Sci. Mater Electron*, 28 (2017) 6529..

27 Suresh G, Sahadevan K, Sambathkumar & Kumaresan *Indian J Pure Appl Phys*, 57 (2019) 196.

28 http://riodbol.ibase.aist.go.jp/sdbs/ (National Institute of Advanced Industrial Science).